

Electron scattering in HCl: An improved nonlocal resonance model

J. Fedor*

Department of Chemistry, Chemin du Musée 9, CH-1700 Fribourg, Switzerland

C. Winstead and V. McKoy

A.A. Noyes Laboratory of Chemical Physics, California Institute of Technology, Pasadena, California 91125, USA

M. Čížek, K. Houfek, P. Kolorenč, and J. Horáček

Institute of Theoretical Physics, Faculty of Mathematics and Physics, Charles University, V Holešovičkách 2, 180 00 Prague 8, Czech Republic

(Received 11 January 2010; published 5 April 2010)

We present an improved nonlocal resonance model for electron-HCl collisions. The short-range part of the model is fitted to *ab initio* electron-scattering eigenphase sums calculated using the Schwinger multichannel method, while the long-range part is based on the *ab initio* potential-energy curve of the bound anion HCl^- . This model significantly improves the agreement of nonlocal resonance calculations with recent absolute experimental data on dissociative electron attachment cross sections for HCl and DCl. It also partly resolves an inconsistency in the temperature effect in dissociative electron attachment to HCl present in the literature. Finally, the present model reproduces all qualitative structures observed previously in elastic scattering and vibrational-excitation cross sections.

DOI: [10.1103/PhysRevA.81.042702](https://doi.org/10.1103/PhysRevA.81.042702)

PACS number(s): 34.80.Ht, 34.80.Gs

I. INTRODUCTION

Resonant electron scattering in hydrogen chloride leads to a variety of phenomena, which makes it a rewarding system to study both experimentally and theoretically. A plethora of structures in various cross sections—dissociative attachment (DA), vibrational excitation (VE), and associative detachment (AD)—have been revealed so far, and their explanation and reproduction have presented a challenge for theoretical models.

Interest in electron-HCl collisions was initiated by the discovery by Rohr and Linder [1] of sharp peaks at threshold in the cross sections for excitation of the $v = 1$ and $v = 2$ vibrational levels. These peaks attained surprisingly large absolute values and showed nearly isotropic angular distributions. Knoth *et al.* [2] observed rotational transitions occurring simultaneously with the $v = 0 \rightarrow 1$ vibrational excitation at the energies of these threshold peaks and reported the angular distributions close to threshold to be nonisotropic. Narrow structures at the thresholds for VE have been also observed by Burrow [3] in measurements of the derivative of the elastic cross section at 180° . Another interesting feature in the VE cross section is the presence of the boomerang vibrational structure reported by Cvejanovic and Jureta [4] and by Schafer and Allan [5] in the $v = 0 \rightarrow 1$ and $v = 0 \rightarrow 2$ excitation functions. This structure was resolved in greater detail in scattering experiments on vibrationally and rotationally cooled HCl by Allan *et al.* [6]; that study also revealed a similar structure in the elastic channel.

Several distinctive features are also seen in the DA collision channel. Steplike structures at vibrational thresholds (Wigner

cusps), caused by interchannel coupling, were reported by Abouaf and Teillet-Billy [7] in the DA cross section. Allan and Wong [8] confirmed these structures and reported a strong dependence of the DA cross section on the target temperature in the range of 330 to 1180 K. The cross sections for the inverse process, associative detachment, revealed steplike structures associated with the rovibrational onsets and steep rises caused by interchannel coupling [9–12].

Several theoretical models have been proposed to provide an explanation of these unusual phenomena. They include the zero-range potential models [13–15], the *R*-matrix formalism [16–18], and models based on projection-operator formalism [19]. The most complete description of the resonance and threshold features observed in low-energy electron-HCl collisions so far has been obtained by the nonlocal resonance model, which belongs to the last class of the approaches listed above. This approach is based on the resonant picture wherein one assumes the existence of a discrete negative ion state that is embedded in the scattering continuum of the electronic ground state of the neutral target molecule. The electronic coupling between the discrete ion state and the scattering continuum is represented by an energy-dependent complex optical potential, with threshold energy dependence given by the strength of the permanent dipole moment. All the free parameters of the model can be determined directly from *ab initio* fixed-nuclei calculations or are adjusted by a least-squares fit to the energy dependencies of the fixed-nuclei eigenphase sums.

The first model for HCl of this type was developed by Domcke and Münder [20]. It described qualitatively all the features observed in various cross sections. This model has been improved by Čížek *et al.* [21] by adding the dependence of the dipole-modified threshold exponent on the internuclear distance and determining the long-range part of the HCl^- potential-energy function from accurate *ab initio* calculations. The model of Čížek *et al.* agreed with experiment better even though they fully adopted the short-range part of the

*Present address: J. Heyrovský Institute of Physical Chemistry, Academy of Sciences of the Czech Republic, Dolejškova 3, CZ-18223 Prague, Czech Republic; juraj.fedor@jh-inst.cas.cz

nonlocal resonance model of Domcke and Mündel [20]. Better agreement was obtained both for the shape of the DA bands and for the VE functions [21]. Additionally, the model of Čížek *et al.* predicted features in the AD spectra that were confirmed by the experiment [11] and even very fine details (outer well resonances and boomerang structures) in the VE spectra. Throughout this paper we will refer to this model as the DMHC model (in Ref. [21] this model was denoted as DMHC-2).

There remain two unsolved discrepancies between the DMHC model and experiment, however: (i) the dependence of the DA cross section on temperature and (ii) the absolute magnitude of the DA cross sections. Discrepancy (i) was revealed by comparing the predictions of the DMHC model with the experiments of Allan and Wong [8], which showed a strong dependence of the shape of the DA cross section on the rotational and vibrational excitation of the target molecules. With increasing temperature, peaks start to appear at lower electron energies because of DA to thermally populated higher rovibrational levels. The DMHC model predicted the general shape of the spectra correctly but underestimated the intensities of the peaks due to vibrationally excited HCl relative to the $v = 0$ peak. Discrepancy (ii) was revealed by the recent measurements of absolute cross sections for DA to hydrogen halides by Fedor *et al.* [22], which showed that the DMHC model overestimates the cross sections for HCl and DCI by factors of 2.5 and 2.8, respectively. These two disagreements were a bit surprising especially in light of the fact that a similarly constructed nonlocal resonance model for HBr [23] agrees very well with both the experimental absolute DA cross sections [22] and the measured DA temperature dependence [24].

The magnitude of the cross section (for each rovibrational state) is a sensitive function of the parameters describing the resonance involved (the resonant width in the local complex potential picture). In Ref. [22], it has been suggested that the reason for the above-mentioned discrepancies of the model with the experiment might be that the description of the resonance in the DMHC model is based on the electron-scattering calculations by Padiál and Norcross [25], which are substantially older than the calculations used for the construction of the model for HBr (Fandreyer *et al.* [26]). In this work, we test this hypothesis by performing elaborate scattering calculations using the Schwinger multichannel method and fitting the nonlocal resonance model for HCl to these calculations. For DA cross sections and DA temperature dependence, the results of the new model agree with the experimental data better than the results of the DMHC model. For VE (where already DMHC worked well) the agreement is equally good.

II. ELECTRON-SCATTERING CALCULATIONS

The elastic electron-scattering cross section was computed within the static-exchange plus polarization approximation using the Schwinger multichannel (SMC) method [27,28] as implemented for parallel computers [29,30]. The ground state of HCl was obtained using the electronic structure package GAMESS [31] at the Hartree-Fock level within a one-electron basis set that incorporated the “augmented correlation-consistent polarized valence double-zeta” (aug-cc-pVDZ) contracted Gaussian basis set of Dunning [32,33], with the $x^2 + y^2 + z^2$ “3s” linear combinations of the Cartesian

d Gaussians excluded. To improve the description of the electronic wave function for the scattering system, additional uncontracted Gaussians, 3 s (exponents 0.6, 0.24, 0.1) and 2 p (exponents 0.727 and 0.141), were placed at each of 32 extra centers. All but two of these centers were arranged in five hexagons about the molecular axis, with hexagons centered on the bond midpoint, on each nucleus, and half a bond length beyond each nucleus. The remaining two centers were placed on the molecular axis, one bond length past each atom. The centers in the two hexagons surrounding the nuclei were located 1.3 Å, or approximately the equilibrium bond length, from the molecular axis, while those in the remaining three hexagons were placed twice as far from the axis. This set of supplemental functions added flexibility to the basis, including a partial description of ϕ (azimuthal quantum number $m = 3$) scattering, without introducing unacceptable numerical linear dependence. Altogether, the one-electron space contained 264 functions, from which we formed the 9 occupied molecular orbitals and 255 modified virtual orbitals (MVOs) [34]; in obtaining the latter, we used a +6 cationic core.

The equilibrium bond length computed with GAMESS [31] at the level of second-order Möller-Plesset perturbation theory in the 6–31G(d) basis set [35–37] was 1.280 Å or 2.419 bohrs. At this bond length, a full scattering calculation was carried out. All 255 doublet configurations formed by antisymmetrizing the Hartree-Fock ground state with one of the MVOs were included in variational space. To describe target polarization effects, we also included closed-channel configurations based on singlet and triplet single excitations from one of the four valence orbitals into low-energy MVOs: the 30 lowest MVOs for singlet-coupled excitations, and the 15 lowest for triplet-coupled excitations. In all there were 43 677 of these closed-channel terms, giving a total dimension for the SMC variational space of 43 932 doublet configuration state functions (CSFs). In practice, separate calculations were carried out for the four irreducible representations of the C_{2v} subgroup of the full $C_{\infty v}$ molecular symmetry group. Because of the hexagonal arrangement of extra centers, the 2B_1 and 2B_2 spaces were not precisely equivalent, nor was the component of ${}^2\Delta$ contained in 2A_1 treated exactly as the component contained in 2A_2 . However, the fact that equivalence was not imposed was useful in assessing convergence of the calculations. From 2.25 to 14 eV, the 2B_1 and 2B_2 contributions to the integral cross section agreed to better than 1%. At lower energies, where the ${}^2B_{1,2}$ cross sections are small, percentage differences increased, but absolute agreement was still good (differences of $\sim 0.05 \times 10^{-16}$ cm² or less), while at higher energies, differences increased from about 2% at 15 eV to about 10% at 30 eV.

At the remaining bond lengths—2.0, 2.1, 2.2, 2.3, 2.5, 2.6, 2.7, 2.8, 2.9, and 3.0 bohrs—calculations were carried out in the same manner, but only for the 2A_1 component of C_{2v} in which the σ^* temporary anion of interest occurs, and with the number of singlet-coupled excitations slightly reduced by using the lowest 29, rather than 30, MVOs as “particle” orbitals. At each bond length, the 2A_1 eigenphase sum was computed from the plane-wave representation $f(\vec{k}_{\text{in}}, \vec{k}_{\text{out}})$ of the scattering amplitude, with $\vec{k}_{\text{in},\text{out}}$ represented on a spherical quadrature grid.

III. NONLOCAL RESONANCE MODEL

A detailed description of the nonlocal resonance formalism has been given elsewhere [19,23]. Here we give only a brief overview in order to introduce the model.

This formalism *a priori* assumes that a temporary resonant state is formed in the electron-molecule collision. This resonant state is described by a square-integrable function $|\varphi_d\rangle$ which is embedded in the scattering continuum of the electronic ground state of the neutral target molecule. The continuum scattering states $|\varphi_\epsilon\rangle$ are orthogonal to $|\varphi_d\rangle$. The Hamiltonian H of such a resonance model including nuclear motion can be written as [19]

$$H = T_N + |\varphi_d\rangle V_d(R) \langle \varphi_d| + \int d\epsilon d\Omega |\varphi_\epsilon\rangle [V_0(R) + \epsilon] \langle \varphi_\epsilon| + \int d\epsilon d\Omega |\varphi_d\rangle V_{d\epsilon}(R) \langle \varphi_\epsilon| + \int d\epsilon d\Omega |\varphi_\epsilon\rangle V_{d\epsilon}^*(R) \langle \varphi_d|. \quad (1)$$

Here, R is the internuclear distance, T_N is the kinetic-energy operator of the nuclei, V_0 is the adiabatic potential energy of the ground electronic state of HCl, V_d is the discrete-state potential, and $V_{d\epsilon}$ is the coupling amplitude between the discrete state and the continuum, $V_{d\epsilon} = \langle \varphi_d | H_{el} | \varphi_\epsilon \rangle$. The solution of the Lippmann-Schwinger equation with the Hamiltonian (1) and the resulting expressions for the electron-scattering cross sections were described in detail in our previous publications [21,23].

The nonlocal resonance model for a given molecule is thus fully specified by three functions $V_0(R)$, $V_d(R)$, and $V_{d\epsilon}(R)$. In the present model, the potential-energy curve of the neutral HCl ground state $V_0(R)$ is fully adopted from the DMHC model [21], i.e., a Morse function with the parameters fitted to the spectroscopic data [see the Appendix for the detailed form of $V_0(R)$]. The form of the discrete-state potential $V_d(R)$ and the discrete-state-continuum coupling element $V_{d\epsilon}(R)$ can be determined by fitting a Breit-Wigner formula with energy-dependent width $\Gamma(\epsilon, R)$ and level shift $\Delta(\epsilon, R)$ [20],

$$\delta(\epsilon, R) = \delta_{\text{bg}}(\epsilon, R) - \tan^{-1} \frac{\frac{1}{2}\Gamma(\epsilon, R)}{\epsilon - V_d(R) + V_0(R) - \Delta(\epsilon, R)}, \quad (2)$$

to the *ab initio* eigenphase sum. Here, the energy-dependent width is related to the discrete-state-continuum coupling element as

$$\Gamma(\epsilon, R) = 2\pi |V_{d\epsilon}|^2, \quad (3)$$

and the level shift is

$$\Delta(\epsilon, R) = \frac{1}{2\pi} \text{P} \int \frac{\Gamma(\epsilon', R)}{\epsilon - \epsilon'} d\epsilon', \quad (4)$$

where P indicates principal value.

For the construction of the present model, we have parametrized the background eigenphase and resonance width as

$$\delta_{\text{bg}} = \frac{\pi}{2} \left(\frac{1}{2} - \alpha(R) \right) + a_{\text{bg}}(R) \epsilon^{\alpha(R)} + b_{\text{bg}} \epsilon, \quad (5)$$

$$\Gamma(\epsilon, R) = g^2(R) [\beta(R) \epsilon]^{\alpha(R)} e^{-\beta(R) \epsilon}. \quad (6)$$

Here, $a_{\text{bg}}(R)$, $b_{\text{bg}}(R)$, $g(R)$, and $\beta(R)$ are smooth functions of R , and $\alpha(R)$ represents the threshold exponent. This parametrization is slightly different from the parametrization of Domcke and Mündel [20], which was used in the DMHC model, and follows the parametrization of the model for HBr [23], which agreed very well with the experimental data. The dependence of the threshold exponent $\alpha(R)$ on the internuclear distance was introduced by Horáček *et al.* [38], adopted in the DMHC model, and retained in the present model. The parameters were fixed as follows: for each of the seven internuclear distances R between 2.0 and 2.6 a.u., we did a five-parameter fit to the *ab initio* eigenphase sums with the parameters g , β , a_{bg} , b_{bg} , and V_d . Afterward, in analogy with construction of the model for HBr [23], linear functions of internuclear distance [with cutoff for $g(R)$] were fitted to the values of the first four parameters, thus yielding analytical expressions for $g(R)$, $\beta(R)$, $a_{\text{bg}}(R)$, and $b_{\text{bg}}(R)$.

The fitting procedure described above properly characterizes the potential of the discrete state V_d in the region of internuclear distances where the additional electron is not bound, i.e., at R smaller than the crossing point $R \simeq 2.6$ a.u. of the neutral HCl and negative ion HCl^- potential-energy curves. To determine V_d at larger internuclear distances, we use the relation of the model parameters and the adiabatic negative ion HCl^- potential-energy curve [21]

$$V_d(R) = V_i(R) - \Delta(V_i(R) - V_0(R), R). \quad (7)$$

The adiabatic potential energy V_i can be obtained from standard quantum chemical calculations. The values of V_d found from relation (7) using data of Åstrand and Karlström [39] for V_i are shown as empty circles in Fig. 1. The same figure contains also the short-range values of the discrete-state potential $V_d(R)$ obtained from the above-mentioned fitting of the eigenphase sums by the Breit-Wigner formula (2). The final functional form of the present model is given in the Appendix and was obtained as the analytical fit to all of these data points.

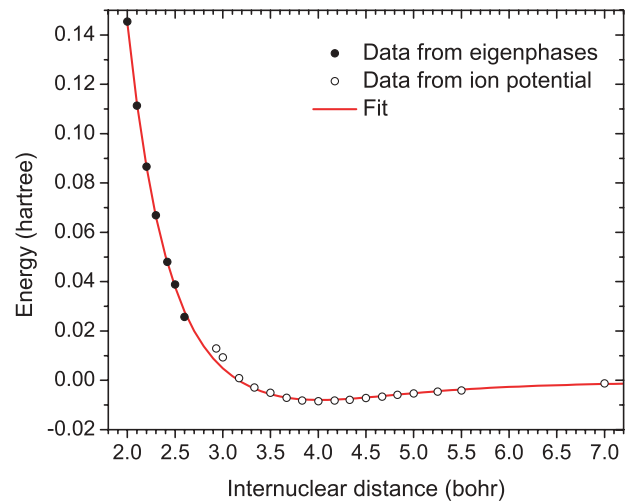


FIG. 1. (Color online) Construction of the discrete-state potential $V_d(R)$. Full circles: data from fitting *ab initio* eigenphase sums; empty circles: data derived from potential-energy curve of Åstrand and Karlström [39]; solid line: final form of $V_d(R)$ as used in the present model.

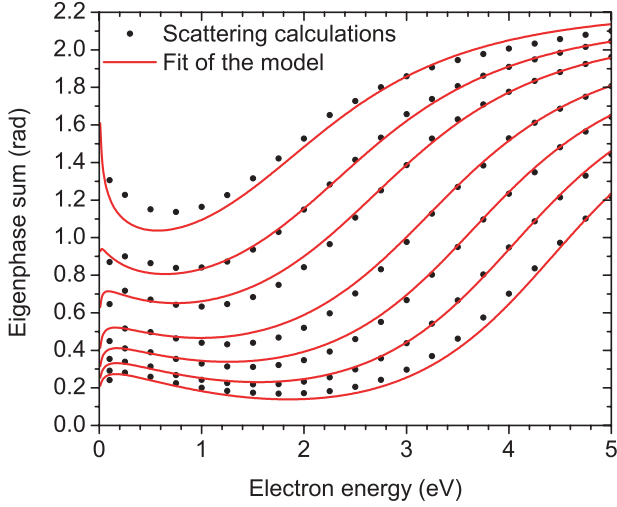


FIG. 2. (Color online) Eigenphase sums for fixed-nuclei electron-HCl scattering. Dots: Schwinger Multichannel method; solid lines: generalized Breit-Wigner formula (2) with the final parameters of the present nonlocal resonance model. Internuclear distances are $R = 2.0, 2.1, 2.2, 2.3, 2.419, 2.5,$ and 2.6 a.u. (from bottom to top).

The determination of this function completes the definition of the nonlocal resonance model.

Figure 2 compares the eigenphase sums for fixed-nuclei scattering obtained from the SMC calculations and from the Breit-Wigner formula (2) with the final set of parameters for the model collected in the Appendix. The fit agrees reasonably well with all data points except for the uppermost curve. This discrepancy is a consequence of the above-mentioned procedure of constructing the model from two separate types of calculations: electron scattering for $R \leq 2.6$ a.u. and adiabatic anion potential for $R > 2.6$ a.u. The smooth connection between the two data sets is problematic as we can see also from Fig. 1: the final smooth curve for $V_d(R)$ does not represent well either the last full circle or the first empty circles. Because the transition region between $R = 2.6$ and 3.0 a.u. is problematic for the *ab initio* calculations, we decided not to consider the scattering data for $R > 2.6$ a.u. or the anion potential data for $R < 3.0$ a.u. in the fitting procedure.

Figure 3 shows the local potential-energy functions of the present model (V_0, V_i, V_d) and their comparison with the DMHC model. The potential-energy curve $V_d(R)$ in the new model is less repulsive. Also the function $\Gamma(\epsilon, R)$ (not shown in the figure) is larger in the new model. Both these facts lead

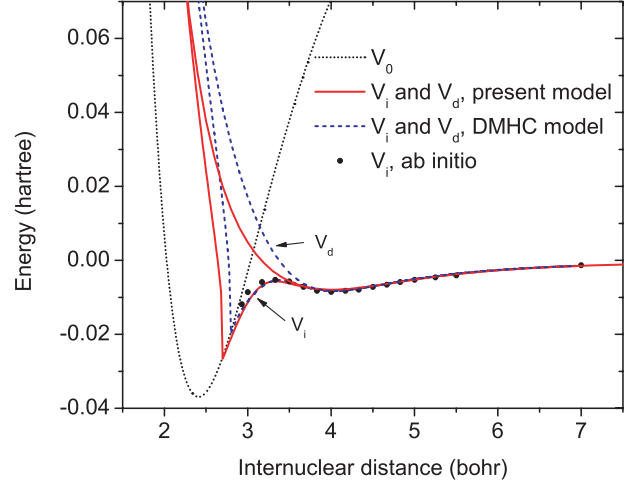


FIG. 3. (Color online) Potential-energy functions relevant in the nonlocal resonance model. Dotted line: ground state of neutral HCl, $V_0(R)$; full lines: discrete-state potential $V_d(R)$ and ion potential $V_i(R)$ of the present model; dashed lines: $V_d(R)$ and $V_i(R)$ of the DMHC model [21]; full circles: *ab initio* HCl⁻ potential of Åstrand and Karlström.

to the expectation that the dissociative cross section will be smaller for the new model and that the isotope effect will be more pronounced (see the discussion in the next section).

IV. RESULTS AND DISCUSSION

A. Dissociative electron attachment

The direct motivation for this work was to improve the quantitative agreement of the DA cross sections calculated from the DMHC model with the recent experimental data of Fedor *et al.* [22]. Because the actual height and shape of the DA peak generally depend on the energy resolution of the electron beam used in the experiment, an energy-integrated cross section σ_I is a more suitable quantity for quantitative comparison. Table I compares the present integrated DA cross sections with those of the previous DMHC model and with experimental and older theoretical cross sections. The experimental values of Fedor *et al.* [22] listed in Table I are larger by 5.7% than the actual values given in Ref. [22], reflecting the introduction of the Knudsen correction to pressure, as discussed by May *et al.* [40]. The experiments were performed at 330 K, and the theoretical cross sections

TABLE I. Energy-integrated dissociative electron attachment cross sections σ_I for HCl and DCl (in units of Å² eV).

Ion	Target	Present model	DMHC [21,41]	Recent expt. [22]	Other expt.	Other theor.
Cl ⁻	HCl	6.28×10^{-2}	14.9×10^{-2}	$(7.24 \pm 1.45) \times 10^{-2}$	3.52×10^{-2} [42]	3.32×10^{-2} [43]
					1.5×10^{-2} [44]	15.0×10^{-2} [18]
					7.4×10^{-2} [45]	
					13.7×10^{-2} [46]	
Cl ⁻	DCl	0.29×10^{-2}	1.25×10^{-2}	$(0.47 \pm 0.095) \times 10^{-2}$	0.704×10^{-2} [42]	0.234×10^{-2} [43]
					6.0×10^{-2} [45]	
$\sigma_I(\text{HCl})/\sigma_I(\text{DCl})$		21.66	11.92	15.40 ± 4.38	5.0 [42] 1.23 [45]	4.19 [43]

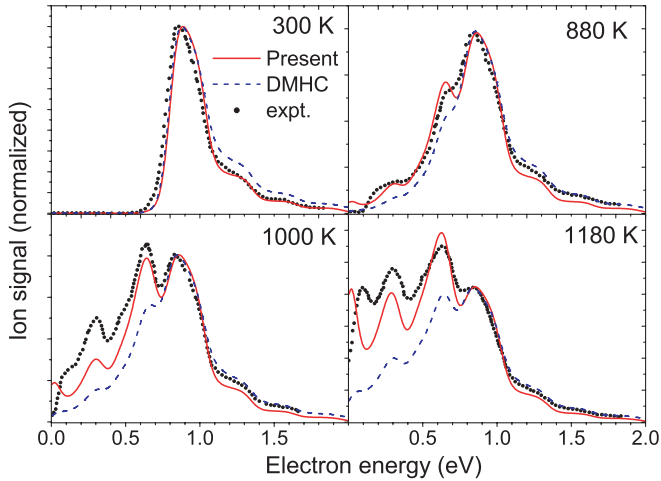


FIG. 4. (Color online) Dissociative electron attachment to HCl at different temperatures of the neutral target. Dots: experimental data of Allan and Wong [8]; full lines: results of the present model; dashed lines: results of the DMHC model. Theoretical curves were convoluted with a Gaussian of 100 meV FWHM. The experimental data were shifted to higher energies by 35 meV. The vertical scales were normalized so that the curves coincide at the maximum of the 0.88 eV peak.

of both models in Table I were evaluated at this temperature. The predictions of the present model are significantly closer to the experimental values than those of the DMHC model. The present prediction for HCl falls within the error bars of the experiment, but the isotopic effect seems to be overestimated by the present calculation.

The shape of the cross section at different temperatures of HCl is compared with the experimental data of Allan and Wong [8] in Fig. 4. For this comparison, both theoretical cross sections were convoluted with a Gaussian of 100 meV full width at half maximum (FWHM), and the experimental data were shifted by 35 meV to higher energies as discussed in Ref. [21]. Since the experimental data are not absolute, the vertical scale was renormalized to the maximum of the 0.88 eV peak. The theoretical curves were obtained by calculating the cross section for each rovibrational level and averaging the results over the Boltzmann distribution of target states.

The shape of the cross section at room temperature is similar in both models and is in good agreement with experiment. On the high-energy flank of the peak, the cross section exhibits steplike features (Wigner cusps) related to the opening of the $0 \rightarrow 3$, $0 \rightarrow 4$, and $0 \rightarrow 5$ vibrational-excitation channels. At elevated temperatures, additional peaks start to appear at lower electron energies. They result from thermal population of higher rotational and vibrational states. As discussed in Refs. [21,24], rotational excitation plays a more important role—the peak growing at 0.63 eV originates from population of the $v = 0$, $J \geq 10$ levels. The threshold energy for DA to these levels lies below the opening energy for the $0 \rightarrow 2$ VE process, which makes the threshold DA cross section for $J \geq 10$ significantly enhanced with respect to that for $J < 10$ (the same effect as Wigner cusps in energy dependence). The peak at 0.29 eV originates from DA to $v = 1$, $J \geq 10$, because the VE $1 \rightarrow 2$ channel is closed at corresponding thresholds.

The relative heights of the peaks at elevated temperatures agree with the experiment better in the present model than in the DMHC model. In Ref. [21], it was suggested that systematic error in the measurement of the temperature by Allan and Wong might have been responsible for the discrepancy between the experiment and the DMHC model. The better agreement of the present model refutes this conjecture.

The better agreement of the present model with the experimental data can be attributed to the larger width function Γ as compared to the previous DMHC model. The dynamics of the dissociative attachment can roughly be understood in the following way: the temporary negative ion is initially formed with the internuclear separation close to the equilibrium internuclear distance of neutral HCl. The subsequent dynamics is the result of the competition between the acceleration of the nuclei toward larger bond length and autodetachment of the electron. The rate of acceleration is controlled by the slope of $V_d(R)$, while the rate of autodetachment is controlled by the magnitude of Γ . Larger Γ thus leads to faster autodetachment, i.e., smaller dissociation probability. The dependence of the DA cross section on the initial vibrational state of the molecule becomes more pronounced for larger Γ , or more precisely, the cross section for DA to excited states gets reduced by smaller factors than the DA cross section for molecules in the ground vibrational state. This leads to a larger reduction of the main peak and a smaller reduction of the side peaks with temperature, as seen in Fig. 4, which improves the agreement of the new calculation with the experimental data.

The remaining discrepancies between the present model and experiment can be understood as imperfections of the present model. We found that the relative heights of DA peaks at elevated temperatures are extremely sensitive to the parameters of the model. This can be attributed to the fact that a small uncertainty in the resonance width Γ will have a large effect on the magnitude of the cross section for each rovibrational level.

B. Vibrational excitation

Figure 5 shows cross sections for $0 \rightarrow v$ vibrational excitation ($v = 1, 2, 3, 4, 5$) for electron energies up to 4 eV. The present results are compared with the DMHC model and the experimental data of Schafer and Allan [5]. The experimental data are not absolute and are scaled so that they agree with the present model for the $0 \rightarrow 2$ cross section near 1 eV. It is important to note that the scaling does not influence the relative normalization of different VE channels. Only the transitions from the rotational ground state $J = 0$ are shown. For comparison to the measurements, both theoretical results were convoluted with a Gaussian of 35 meV FWHM.

Both models qualitatively reproduce the shape of the excitation curves: the occurrence of threshold peaks for the $0 \rightarrow 1$ and $0 \rightarrow 2$ channels and structures in the broad resonance region. Furthermore, the new calculation shows very good agreement with the experimental data close to threshold. For energies more than 1 eV above threshold in each channel, the agreement gets much worse. As we saw in previous section, the fitting procedure determining the nonlocal resonance model from the fixed-nuclei electronic calculations was problematic in the region where the electron-scattering and

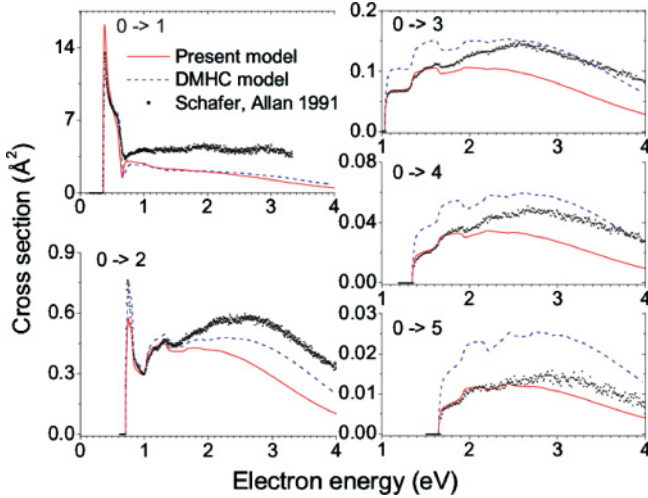


FIG. 5. (Color online) Vibrational-excitation cross sections. Dots: experimental data of Schafer and Allan [5]; full lines: results of the present model; dashed lines: results of the DMHC model. Theoretical curves were convoluted with a Gaussian of 35 meV FWHM. The experimental data were scaled so that they agree with the present model for the $0 \rightarrow 2$ cross section near 1 eV.

bound-anion-state data are joined together. We expect that this will have a smaller influence for smaller energies. An additional source of error is our neglect of the role of the background term in the VE process [47]. The present model also does not consider the second electronic state of HCl^- , which may be important close to the $\text{H}^- + \text{Cl}$ threshold.

Figure 6 shows part of the elastic and $0 \rightarrow 1$ cross sections on an expanded scale in comparison with the measurements performed on vibrationally and rotationally cooled HCl [6,48]. As discussed in more detail elsewhere [6,49], the sharp structures in the cross section reflect the details of the long-range $\text{H} + \text{Cl}^-$ potential and are also closely related to the long-lived HCl^- states [50]. The overall shape of the structures

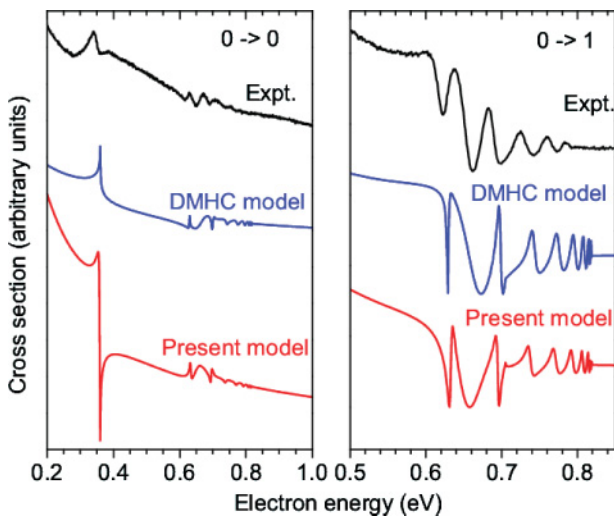


FIG. 6. (Color online) Relative elastic cross sections (left panel) and relative $0 \rightarrow 1$ vibrational-excitation cross sections (right panel) in the energy range where oscillatory structures are found. Experimental data are from Ref [6].

remains unchanged in the new calculation, and the degree of agreement with the experiment remains very good, considering the effect of finite temperature on the experiment and the neglect of the (smooth) background term in the theoretical calculation.

V. CONCLUSIONS

We have carried out fixed-nuclei electron-HCl calculations using the Schwinger multichannel method, and the eigenphase sums obtained from these calculations were used to construct an improved nonlocal resonance model. Other basic components of the model—the long-range ion potential and the neutral HCl potential—were kept the same as in the DMHC model of Ref. [21].

The quantitative dissociative electron attachment cross sections resulting from the present model are in much better agreement with recent experiments of Fedor *et al.* [22] than the results of the DMHC model. The present model also resolves, to a large degree, a contradiction in the literature: it improves the agreement with the experimental data on the DA temperature dependence [8]. The qualitative features in the elastic and vibrational-excitation cross sections were already described adequately by the old model, and the new model describes them equally well.

ACKNOWLEDGMENTS

We thank M. Allan, Fribourg, for fruitful discussions and valuable comments. This work has been supported by the Swiss National Science Foundation (Contract No. 200020-113599/1), COST Action CM0601, COST Action OC09079, Grant No. GACR 202/07/0833 of the Czech Science Foundation, and Záměr MŠMT No. MSM0021620860. The work of V.M. and C.W. was supported by the Chemical Sciences, Geosciences and Biosciences Division, Office of Basic Energy Sciences, Office of Energy Science, US Department of Energy, and made use of the Jet Propulsion Laboratory’s Supercomputing and Visualization Facility.

APPENDIX: DESCRIPTION OF THE PRESENT MODEL

Atomic units are used unless stated otherwise.

The model is fully specified by three functions: the neutral potential $V_0(R)$, the discrete-state potential $V_d(R)$, and the discrete-state coupling element $V_{d\epsilon}(R)$ [related to the energy-dependent width $\Gamma(R, \epsilon)$ via Eq. (3)].

For the potential of neutral HCl, we used the same Morse function as in the DMHC model:

$$V_0(R) = 0.169414e^{-1.002(R-R_0)}(e^{-1.002(R-R_0)} - 2) + E_a, \quad (\text{A1})$$

where the equilibrium distance is $R_0 = 2.409$ and the electron affinity of the chlorine atom is $E_a = 3.605 \text{ eV} = 0.132481$.

The form of the discrete-state potential (solid line in Fig. 1) is

$$V_d(R) = 0.0546277e^{-2.45832(R-R_0)} - \frac{2.25}{[(R - 3.67061)^2 + 52.3152]^2 - 2500}. \quad (\text{A2})$$

The energy-dependent resonance width is

$$\Gamma(\epsilon, R) = g^2(R)[\beta(R)\epsilon]^{\alpha(R)}e^{-\beta(R)\epsilon}. \quad (\text{A3})$$

Together with a_{bg} and b_{bg} from Eq. (2), $g(R)$ and $\beta(R)$ were determined from fits to the *ab initio* eigenphase sums to be

$$g(R) = 0.749083(1 - 0.166537R)[1 + e^{4.2(R-3.18)}]^{-1}, \quad (\text{A4})$$

$$\beta(R) = 0.43150R + 5.80996, \quad (\text{A5})$$

$$a_{\text{bg}}(R) = 0.807215R - 4.3830, \quad (\text{A6})$$

$$b_{\text{bg}}(R) = 1.269710. \quad (\text{A7})$$

The threshold exponent $\alpha(R)$ was kept the same as in DMHC model,

$$\alpha(R) = \frac{1}{2} + a_1M^2 + a_2M^4 + a_3M^6 + a_4M^8, \quad (\text{A8})$$

with

$$M(R) = M_0(1 + R)^3 \left(1 + \sum e_i R^i\right)^{-1}. \quad (\text{A9})$$

The parameters a_i , e_i , and M_0 are

$$\begin{array}{lll} a_1 = -0.101157, & M_0 = 1.09333, & e_4 = 1.829, \\ a_2 = -0.0014833, & e_1 = 1.897, & e_5 = -4.137, \\ a_3 = -0.007486, & e_2 = 0.871, & e_6 = 13.886, \\ a_4 = -0.003735, & e_3 = 1.465, & e_7 = 0.416. \end{array}$$

-
- [1] K. Rohr and F. Linder, *J. Phys. B* **9**, 2521 (1976).
 [2] G. Knoth, M. Rädle, M. Gote, H. Erhardt, and K. Jung, *J. Phys. B* **22**, 299 (1989).
 [3] P. D. Burrow, *J. Phys. B* **7**, L385 (1974).
 [4] S. Cvejanović and J. Jureta, in Abstracts of the 3rd European Conference on Atomic and Molecular Physics, Bordeaux, 1989 (unpublished), p. 638.
 [5] O. Schafer and M. Allan, *J. Phys. B* **24**, 3069 (1991).
 [6] M. Allan, M. Čížek, J. Horáček, and W. Domcke, *J. Phys. B* **33**, L209 (2000).
 [7] R. Abouaf and D. Teillet-Billy, *J. Phys. B* **10**, 2261 (1997).
 [8] M. Allan and S. F. Wong, *J. Chem. Phys.* **74**, 1687 (1981).
 [9] T. S. Zwier, M. M. Maricq, C. J. S. M. Simpson, V. M. Bierbaum, G. B. Ellison, and S. R. Leone, *Phys. Rev. Lett.* **44**, 1050 (1980).
 [10] J. P. Gauyacq, *J. Phys. B* **15**, 2721 (1982).
 [11] S. Živanov, M. Allan, M. Čížek, J. Horáček, F. A. U. Thiel, and H. Hotop, *Phys. Rev. Lett.* **89**, 073201 (2002).
 [12] S. Živanov, M. Čížek, J. Horáček, and M. Allan, *J. Phys. B* **36**, 3513 (2003).
 [13] L. Dubé and A. Herzenberg, *Phys. Rev. Lett.* **38**, 820 (1977).
 [14] J. P. Gauyacq and A. Herzenberg, *Phys. Rev. A* **25**, 2959 (1982).
 [15] W. Vanroose, C. W. McCurdy, and T. N. Rescigno, *Phys. Rev. A* **68**, 052713 (2003).
 [16] I. I. Fabrikant, *Z. Phys. D* **3**, 401 (1986).
 [17] L. A. Morgan, P. G. Burke, and C. J. Gillan, *J. Phys. B* **23**, 99 (1990).
 [18] I. I. Fabrikant, S. A. Kalin, and A. K. Kazansky, *J. Chem. Phys.* **95**, 4966 (1991).
 [19] W. Domcke, *Phys. Rep.* **208**, 97 (1991).
 [20] W. Domcke and C. Mündel, *J. Phys. B* **18**, 4491 (1985).
 [21] M. Čížek, J. Horáček, and W. Domcke, *Phys. Rev. A* **60**, 2873 (1999).
 [22] J. Fedor, O. May, and M. Allan, *Phys. Rev. A* **78**, 032701 (2008).
 [23] M. Čížek, J. Horáček, A.-Ch. Sergenton, D. B. Popović, M. Allan, W. Domcke, T. Leininger, and F. X. Gadea, *Phys. Rev. A* **63**, 062710 (2001).
 [24] J. Fedor, M. Cingel, J. D. Skalný, P. Scheier, T. D. Märk, M. Čížek, P. Kolorenč, and J. Horáček, *Phys. Rev. A* **75**, 022703 (2007).
 [25] N. T. Padial and D. W. Norcross, *Phys. Rev. A* **29**, 1590 (1984).
 [26] R. Fandreyer, P. G. Burge, C. A. Morgan, and C. J. Gillan, *J. Phys. B* **26**, 3625 (1993).
 [27] K. Takatsuka and V. McKoy, *Phys. Rev. A* **24**, 2473 (1981).
 [28] K. Takatsuka and V. McKoy, *Phys. Rev. A* **30**, 1734 (1984).
 [29] C. Winstead and V. McKoy, *Adv. At., Mol., Opt. Phys.* **36**, 183 (1996).
 [30] C. Winstead and V. McKoy, *Comput. Phys. Commun.* **128**, 386 (2000).
 [31] M. W. Schmidt *et al.*, *J. Comput. Chem.* **14**, 1347 (1993).
 [32] T. H. Dunning Jr., *J. Chem. Phys.* **90**, 1007 (1989).
 [33] R. A. Kendall, T. H. Dunning Jr., and R. J. Harrison, *J. Chem. Phys.* **96**, 6796 (1992).
 [34] C. W. Bauschlicher, *J. Chem. Phys.* **72**, 880 (1980).
 [35] R. Ditchfield, W. J. Hehre, and J. A. Pople, *J. Chem. Phys.* **54**, 724 (1971).
 [36] P. C. Hariharan and J. A. Pople, *Theor. Chim. Acta* **28**, 213 (1973).
 [37] M. M. Francl, W. J. Pietro, W. J. Hehre, J. S. Binkley, M. S. Gordon, D. J. DeFrees, and J. A. Pople, *J. Chem. Phys.* **77**, 3654 (1982).
 [38] J. Horáček, M. Čížek, and W. Domcke, *Theor. Chem. Acc.* **100**, 31 (1998).
 [39] P.-O. Åstrand and G. Karlström, *Chem. Phys. Lett.* **175**, 624 (1990).
 [40] O. May, J. Fedor, and M. Allan, *Phys. Rev. A* **80**, 012706 (2009).
 [41] J. Horáček, M. Čížek, P. Kolorenč, and W. Domcke, *Eur. Phys. J. D* **35**, 225 (2005).
 [42] R. Azria, L. Roussier, R. Paineau, and M. Tronc, *Rev. Phys. Appl.* **9**, 469 (1974).
 [43] D. Teillet-Billy and J. P. Gauyacq, *J. Phys. B* **17**, 4041 (1984).
 [44] I. S. Buchelnikova, *Sov. Phys. JETP* **8**, 783 (1959).
 [45] L. G. Christophorou, R. N. Compton, and H. W. Dickson, *J. Chem. Phys.* **48**, 1949 (1968).
 [46] O. J. Orient and S. K. Srivastava, *Phys. Rev. A* **32**, 2678 (1985).
 [47] K. Houfek, T. N. Rescigno, and C. W. McCurdy, *Phys. Rev. A* **77**, 012710 (2008).
 [48] M. Čížek, J. Horáček, M. Allan, and W. Domcke, *Czech. J. Phys.* **52**, 1057 (2002).
 [49] K. Houfek, M. Čížek, and J. Horáček, *Chem. Phys.* **347**, 250 (2008).
 [50] M. Čížek and J. Horáček, *Int. J. Mass Spectrom.* **280**, 149 (2009).